A Novel Dual Rotor Flux-Bidirectional-Modulation Machine for Hybrid Electrical Vehicles

Yunchong Wang, Shuangxia Niu, W. N. Fu, and S. L. Ho

The Hong Kong Polytechnic University, Hong Kong

A novel brushless and gearless power split system is presented in this paper. The proposed system offers an electric solution for continuously variable transmission of the hybrid electrical vehicles (HEV). The key is to use a doubly fed flux bidirectional modulation machine with dual electric port and dual mechanical port to realize the power combination and split in HEV. This electric continuously variable transmission (E-CVT) system integrates the merits of the dual rotor machine and the flux modulation machine and enjoys additional benefits such as high torque density and low cost partial-scale converter. The operation principle, flux modulation principle and steady performance of the machine are investigated. Time stepping finite element method (TS-FEM) is used to analyze the dynamic performance of the proposed system. The prototype is fabricated and the experimental results verify the correctness of the mathematical model and simulation results.

***Inndex Terms*—E-CVT, finite element method, flux modulation, hybrid electrical vehicle.**

I. Introduction

Due to the rising concerns of the environmental issues and energy crisis, alternative energy vehicles have been a popular field for researchers. With excellent energy efficiency and outstanding driving performance, hybrid electric vehicles (HEVs) have obtained great commercial success in the last decade [1-4]. Generally, the HEVs are classified into three types which are the series hybrid vehicles, the parallel hybrid vehicles and the series-parallel hybrid topology. The series-parallel hybrid topology can eliminate the drawbacks of series hybrid and parallel hybrid topology and provides improved energy conversion performance. As the most famous HEV, Toyota Prius adopts the series-parallel topology and use a planetary gear system to realize the power splitting and combination [5], [6]. The planetary gear system is also named as continuously variable transmission (CVT) system. It is an important and necessary component in advanced series-parallel hybrid electrical vehicles, which acts as a power-splitting unit to ensure the optimal operation of the internal combustion engine (ICE) regardless of the speed variations of the vehicle. However, the planetary gear also brings some defects such as low mechanical reliability, audible noise and high maintenance cost.

To overcome the drawback of the mechanical gear, the concept of electrical continuously variable transmission (E-CVT) system is proposed [7-10]. In the E-CVT system, the planetary gear is superseded by a dual rotor machine (DRM) [11-15]. Using the DRM, the power windings on both stator and inner rotor account for the power splitting and combination. Two rotors provide the speed difference between the ICE and wheels. Therefore the DRM can realize the power splitting and combination requirement of the HEV without a planetary gear. The major drawback of the E-CVT system using conventional DRM is the additional unreliability caused by the brushes and slip-rings. For the conventional DRM, the rotor winding is employed to split the power of the ICE. Therefore, the brushes and slip-rings are essential and bring additional unreliability and maintenance cost.

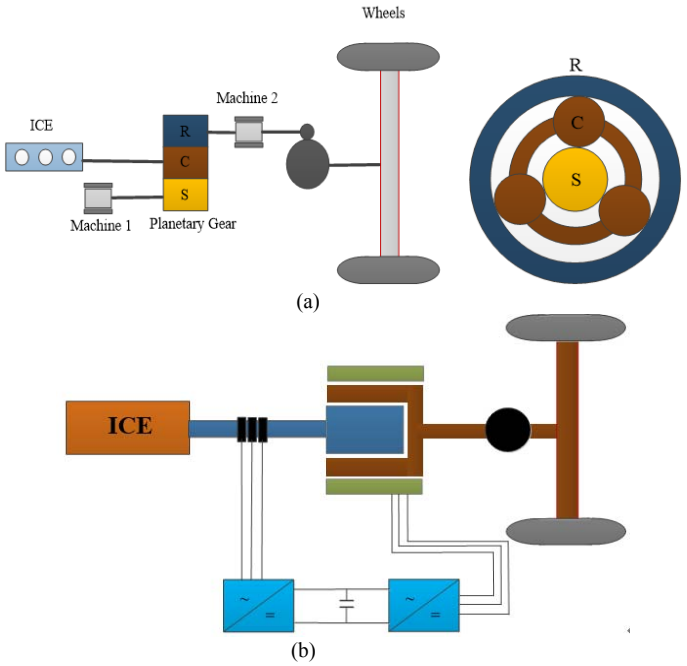

Fig. 1 Basic configuration of the E-CVT systems for HEVs. (a) E-CVT system with a planetary gear. (b) E-CVT system with a dual rotor machine.

In this paper, a novel dual rotor machine with flux modulation structure is proposed and named as dual rotor flux bidirectional modulation machine (DR-FBMM). The flux modulation machine (FMM) is also named as vernier machine or magnet gear machine. The concept of the vernier machine is first proposed by [16] and the magnetic gear using harmonic flux is presented by [17]. In [18], the principles of these two structures are proven to be the same. In both structures, the flux modulation effect is employed to amplify the torque density. Therefore, the FMM is very suitable for the high torque density, directly driving system.

In [19], a flux-modulated double-rotor machine was analyzed and designed for the HEVs. Compared with the conventional DRM, the novel flux modulation machine successfully gets rid of the brushes and slip-rings and particularly appropriates for the HEVs. In [20], an approved machine with complementary structure is proposed and the

complementary design reduces the cogging torque significantly. However, an additional regulating PM machine is needed to decouple the ICE torque and the wheel torque [19]. To integrate the regulating machine into a flux modulation machine, the DR-FBMM is presented. It is used as the core component in E-CVT system for HEV application and realizes the gearless and brushless power split and combination.

The operation principle of the DR-FBMM is analyzed and the control strategy is designed in this paper. The time step finite element method (TS-FEM) is used to verify the mathematical model. The prototype of the DR-FBMM is fabricated and the experimental result is given.

II. BASIC CONFIGURATION AND OPERATION PRINCIPLE

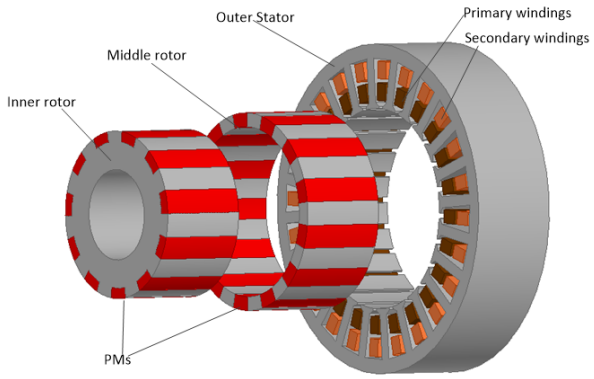

Fig. 2 Basic topology of the proposed DRFMM system

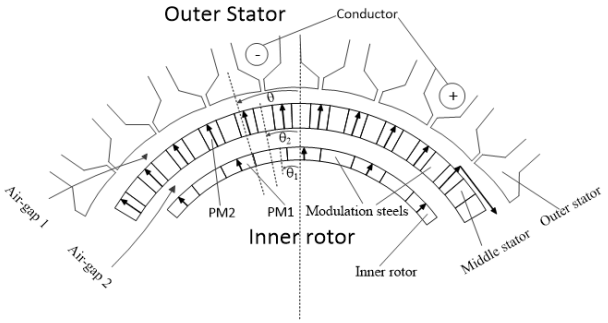

Fig. 3 Portion of a flux modulation magnetic gear.

The basic topology of the DR-FBMM is shown in Fig. 2 The middle rotor of the DR-FBMM is directly connected with the vehicle wheels and the inner rotor coupled with the ICE. There are two sets of 3-phase windings on the stator. The inner winding couples with the modulated field and splits the power of the ICE. The outer winding and the outer rotor comprise a permanent magnet synchronous machine which can enhance the output torque and work as a generator to charge the battery. Moreover, the starting and acceleration performance of HEVs can also be improved with this additional set of windings.

In [21], the operation principle of conventional Vernier permanent magnet machines (VPMM) is illuminated. Based on the mathematical model of the VPMM, the operation principle of the flux modulation machine is derived.

TABLE I
PARAMETERS OF PROPOSED MOTOR

Item	Value
Stator out diameter	240mm
Axial length	65mm
Middle rotor pole pairs (N_1)	13
Middle rotor rated torque	75Nm
Inner rotor pole pairs (N_s)	11
Inner rotor rated torque	45Nm
Rated speed of the middle rotor	2000rpm
Rated speed of the inner rotor	1000rpm
Number of stator slot	24
Number of primary winding pole pair	2
Number of second winding pole pair	13
Primary winding turns per slot	50
Second winding turns per slot	60
Air-gap length	1mm
Magnetic remanence	1.2T

Portion of the DR-FBMM is shown in Fig. 2. There are two sets of modulation groups in the DR-FBMM. As shown in Fig. 3 the inner rotor PMs, the middle rotor steels and the primary windings on the stator consist of the first modulation group. The inner rotor teeth, middle rotor PMs and the primary windings consist of the second modulation group. Both of the modulation groups follow the principle of the flux modulation machine. Table I lists the parameters of the prototype.

In the following, the first modulation group is selected as an example to illuminate the operation principle of the flux modulation effect.

N_1 and N_s are the pole-pair number of the inner rotor PMs and the pieces of middle rotor modulation steels respectively. N_2 is the pole-pair number of the primary windings. θ, θ_1 and θ_2 are the angular position in the air gap, the inner rotor position and the middle rotor position, respectively. ω_1 is the mechanical speed of the inner rotor and ω_2 is the mechanical speed of the middle rotor. The fundamental component of magnetic motive force (MMF) of the inner rotor PMs, $F_{PM1}(\theta,\theta_1)$ and the magnetic circuit permeance of the air gap, $P(\theta)$ can be expressed as:

$$F_{PM1}(\theta,\theta_1)=F_1\cos[N_1(\theta-\theta_1)] = \frac{4}{\pi}\frac{h_m}{\mu_m}B_r\cos[N_1(\theta-\theta_1)] \quad (1)$$

$$P(\theta)=P_0-P_1\cos N_s(\theta-\theta_2) \quad (2)$$

$P(\theta)$ is the permanence induced by the flux modulation effect of the modulation steels. P_0 and P_1 are experiential coefficients. According to (1) and (2), the air gap flux density is shown as,

$$B(\theta,\theta_1) = F_{PM1}(\theta,\theta_1)P(\theta) = \frac{4}{\pi}\frac{h_m}{\mu_m}B_r\cos N_1(\theta-\theta_1)[P_0-P_1\cos N_s(\theta-\theta_2)]$$

$$= \frac{4}{\pi}\frac{h_m}{\mu_m} B_r \begin{Bmatrix} P_0 \cos N_1(\theta - \theta_1) \\ -\frac{P_1}{2}\cos[(N_1 - N_s)\theta - (N_1\theta_1 - N_s\theta_2)] \\ -\frac{P_1}{2}\cos[(N_1 + N_s)\theta - (N_1\theta_1 + N_s\theta_2)] \end{Bmatrix} \quad (3)$$

The flux linkage within one pole range of the primary windings due to the outer rotor PM is given as,

$$\begin{aligned} \varphi(\theta_1) &= r_{g2} l_m \int_0^{\pi/N_2} B(\theta, \theta_1) d\theta \\ &= r_{g2} l_m \frac{4}{\pi}\frac{h_m}{\mu_m} B_r \left\{ \frac{P_0}{N_1} \sin N_1(\theta - \theta_1) \right. \\ &\quad - \frac{P_1}{2(N_1 - N_s)} \sin[(N_1 - N_s)\theta - (N_1\theta_1 - N_s\theta_2)] \\ &\quad \left. - \frac{P_1}{2(N_1 + N_s)} \sin[(N_1 + N_s)\theta - (N_1\theta_1 + N_s\theta_2)] \right\} \Big|_0^{\frac{\pi}{N_2}} \end{aligned} \quad (4)$$

When the pole-pair number of outer rotor equals to the pole-pair number of inner rotors, namely $N_1 = N_2$, the flux density due to the flux modulation effect with $N_1 \pm N_s$ is negligible and there is no gear effect between the two rotors. For the flux modulation machines, P_0 is much smaller than P_1 and the pole pair numbers should satisfy the relationship $N_1 - N_s = -N_2$. Therefore, Eq. (4) can be rewritten as:

$$\varphi(\theta_1) = r_{g2} l_m \frac{4}{\pi}\frac{h_m}{\mu_m} B_r \frac{P_1}{N_2} \sin(N_1\theta_1 - N_s\theta_2) \quad (5)$$

The back-EMF of the primary windings is

$$\begin{aligned} e(t) &= \frac{d\varphi(\theta_1)}{dt} \\ &= r_{g2} l_m \frac{4}{\pi}\frac{h_m}{\mu_m} B_r \frac{P_1}{N_2} (N_1\omega_1 - N_s\omega_2) \sin[(N_1\omega_1 - N_s\omega_2)t] \end{aligned} \quad (6)$$

For the proposed DF-FBMM, the outer rotor PM poles of the magnetic gear are replaced by the stator windings and permanent magnets (PMs) and modulation steels are alternatively arranged on the middle and inner rotors. The frequency of the back-EMF of the primary windings is governed by the speed of the two rotors as:

$$f_p = N_1\omega_1 - N_s\omega_2 \quad (7)$$

Eq.(7) shows that the frequency of the primary windings is determined by both the speed of the inner rotor PMs and the speed of the middle rotor steels. For the second flux modulation groups, the operation principle is similar to the first group.

To enhance the output torque of the middle rotor which directly connects with the middle rotor and realize the function of ISG, an additional winding is planted in the outer stator slots and couples with the middle rotor.

III. FEM MODEL AND CONTROL STRATEGY SIMULATION

A. FEM model simulation

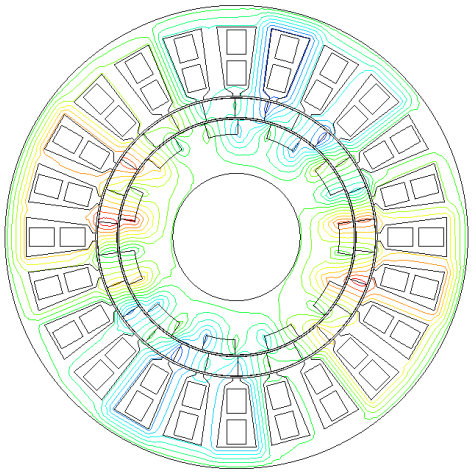

Fig. 4 Flux distribution of the DR-FMM with full-load

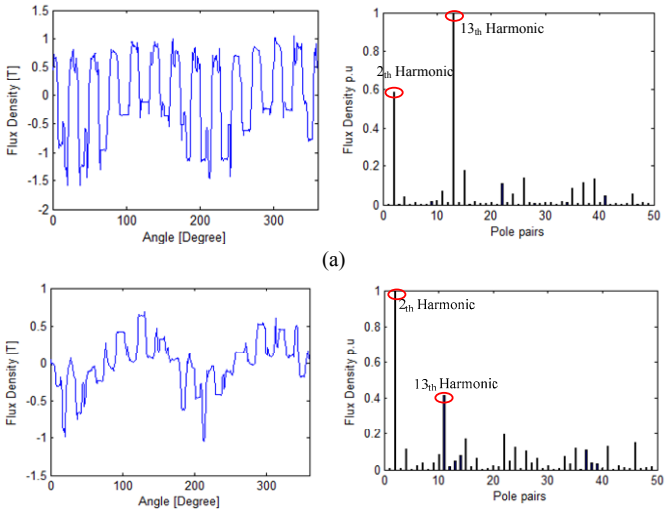

Fig. 5 Flux density distribution in the stator air-gap. (1) The flux density excited by the middle rotor PMs. (2) The flux density excited by the inner rotor PMs.

The flux distribution in the proposed prototype is simulated with the finite element method and shown in Fig. 4. Fig. 5 shows the flux density excited by the middle rotor PMs and inner motor PMs. The middle rotor adjacent to the stator winding induces a field containing numerous space harmonics. The 13_{th} harmonic is the largest one and is useful for the energy conversion between the middle rotor and the secondary winding. The 2_{th} harmonic is smaller than the 13_{th} harmonic but much larger than other harmonics. It accounts for the coupling between the primary winding and the middle rotor. The inner rotor only couples with the primary winding through the 2_{th} harmonic and it is obviously larger than other harmonics. The back-EMF of the windings are shown in Fig. 6, when the rotors are at the rated speed, 1000 rpm for the middle rotor and 2000rpm for the inner rotor. Fig. 4 (a) shows the frequency of the primary winding is 150Hz which excellently

agree with the (7) and the effectiveness of the mathematical model is proved.

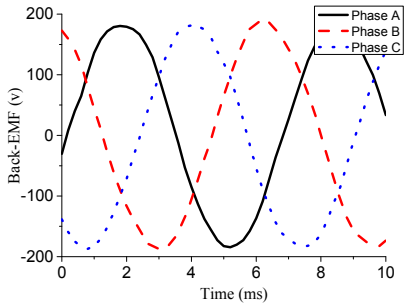

(a)

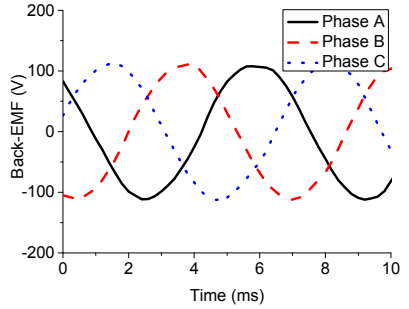

(b)

Fig. 6 No load back-EMF of the primary winding and secondary winding

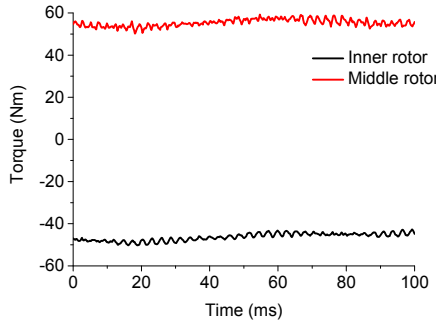

(a)

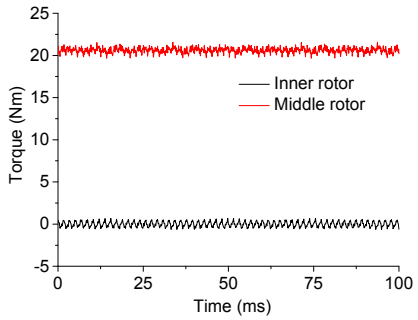

(b)

Fig. 7. The electrical torque of the two rotors: (a) Torque due to the primary windings with 12A current (b) Torque due to the secondary windings with 8A current

The electrical torque of the two rotors is shown in Fig.7. Fig. 7(a) is the steady torque due to the primary windings with 12 A current. The electrical torque due to the secondary windings with 6A is shown in Fig. 7(b). The primary winding couples with both rotors. Therefore, the primary winding current induces torque on two rotors. The average torque of the inner rotor is 45Nm and the outer rotor rated torque induced by the primary winding is 55Nm. The secondary winding couples with the middle rotor individually and the rated torque with 8A current is 20Nm.

B. Control strategy simulation

Fig. 8 shows the control system configuration of the DR-FBMM. The inner rotor with speed control is connected with the engine. The speed control of the inner rotor realizes the optimal operation of the engine. The middle rotor is connected to the wheels and couples with both primary winding and secondary winding. The torque control of the secondary winding is applied to regulate the output torque of the middle rotor.

According to (5), (6) and (7), the primary winding couples with both rotors and the field angle θ_s is calculated by the positions of both rotors. Based on the feedback of the two rotor positions, the FOC control strategy with $i_d = 0$ can be applied for the inner winding control. For the secondary winding, it couples with the middle rotor separately. The conventional FOC control strategy is used for the torque control of the middle rotor.

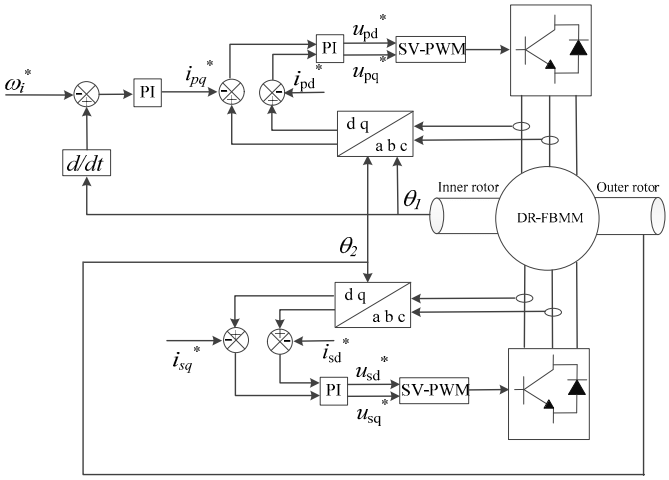

Fig. 8. Schematic of the control system configuration for the DR-FBMM

Fig. 9 shows the simulation result of the control system. In the simulation, the outer rotor is assumed to be run at a constant speed 500rpm and the inner rotor speed is controlled by the primary winding. At 0s, the reference value of the inner rotor speed is set as 650rpm and the load torque on the inner rotor is 5Nm. At 0.4s, the load torque steps to 10Nm, there is a small ripple of the inner rotor speed which is caused by this torque step and the current follows the changes of the load torque. At 0.8s, the reference speed of the inner rotor steps from 650rpm to 950rpm. The simulation result shows the control system owns excellent speed and torque tracking capability. The speed control of the primary winding can ensure the inner rotor operate at the optimal load point of the ICE.

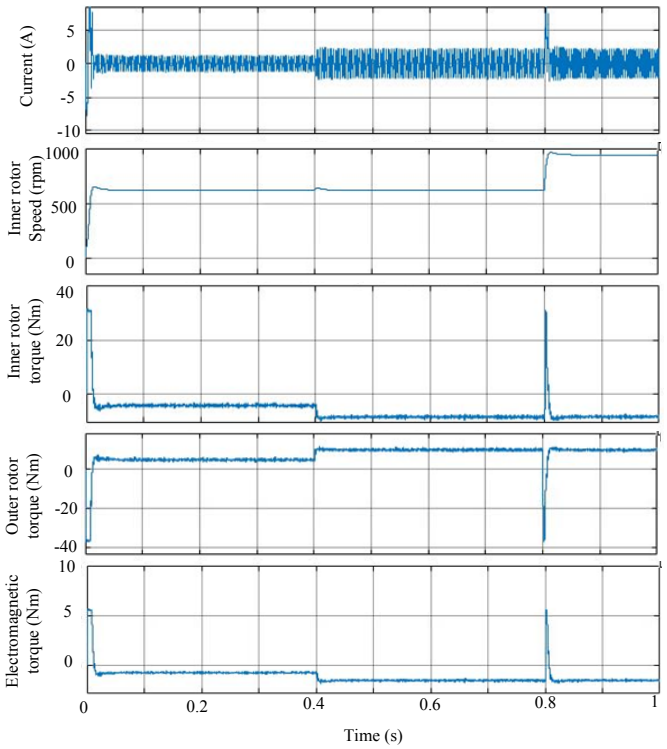

Fig. 9. Simulation results of the control system for the DR-FBMM

IV. EXPERIMENTAL IMPLEMENTATION AND RESULT

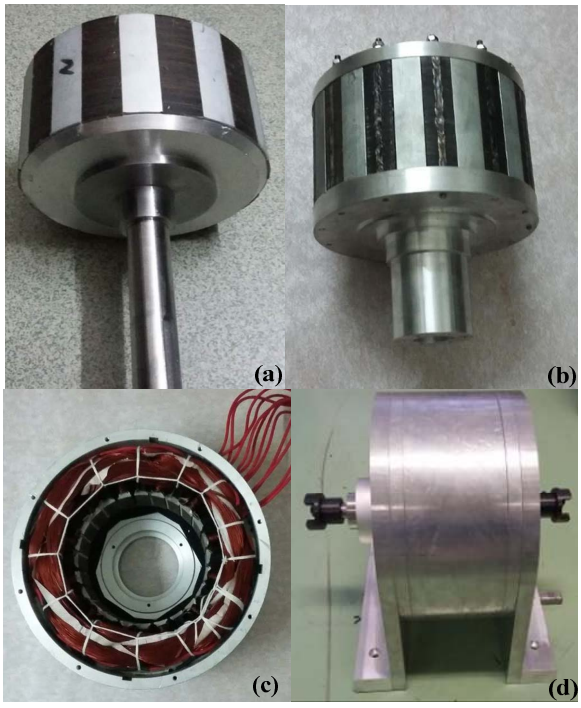

Fig. 11. Photograph of the proposed DR-FBMM. (a) The inner rotor. (b) The middle rotor. (c) The stator and windings. (d) The proposed DR-FBMM

To testify the machine model and the simulation results. A prototype of the DR-FBMM is fabricated as shown in Fig. 11. The test bench uses two servo motors to simulate the functions of ICE and wheel load. The no-load back-EMF waveform of the primary winding and secondary winding is shown in Fig.12. The speeds of the rotors are similar to the condition of FEM simulation mentioned above in fig. 6. The test results shows excellent agreements with the simulation results for both primary winding and secondary winding.

Fig 13 and fig 14 show the simulation results of the power splitting and combination. In the fig 13, the inner rotor connects with the ICE is under speed close-loop control and the input torque is hold by the ICE at a constant value. For the hill-up or acceleration operation mode, the secondary winding is fed by current with $i_q > 0$. In this mode, the power flows from battery to the wheels through both windings. For the braking operation mode, the secondary winding is fed by current with $i_q < 0$ and the power flow back to the battery through the secondary winding. In the fig 14, the load torque is assumed as a constant value. The q-axis current of the secondary winding varies from positive to negative which means the battery power flowing direction changes from output to input. When the battery outputs powers to the wheel load, the output torque of the ICE will decrease to keep the load torque as a constant value, otherwise the ICE will output more power to charge the battery through the secondary winding. This experiment results proves the secondary winding can regulate the working load of the ICE while the speed of the ICE can be controlled by the primary winding with close-loop speed control. Therefore, the E-CVT system with a DR-FBMM can realize the optimal operation of the ICE.

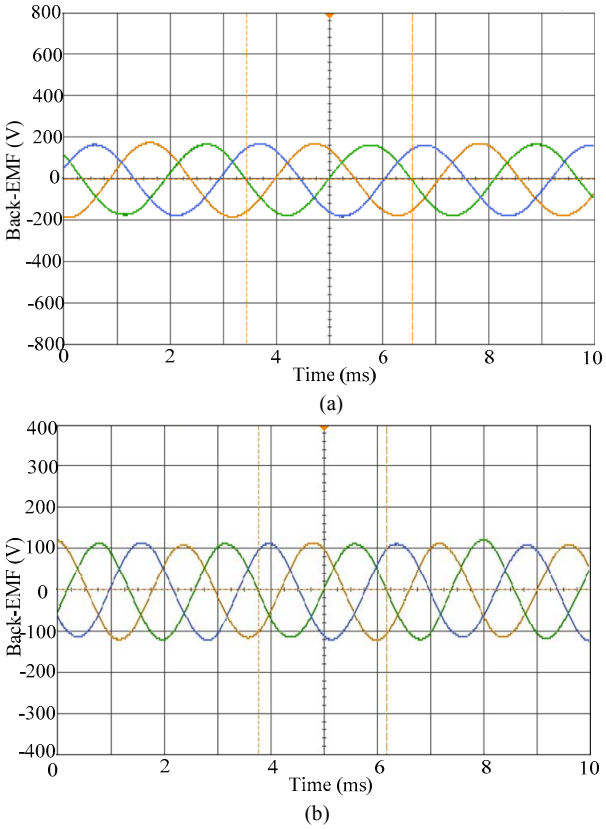

Fig. 12. No load Back-EMF waveform. (a) The primary winding back-EMF waveform. (b) The secondary winding back-EMF waveform.

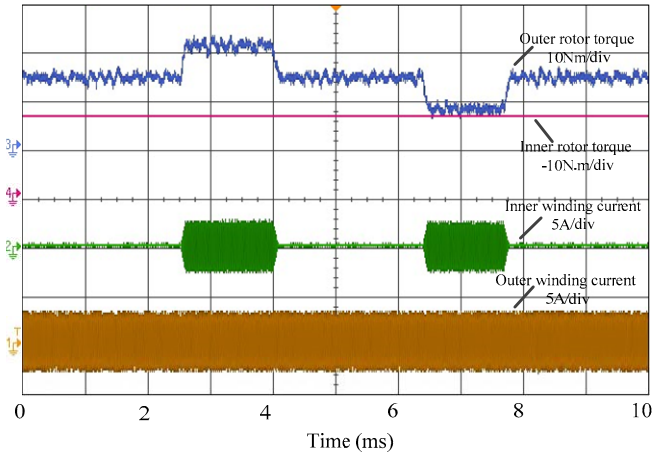

Fig. 13. Simulation results of the inner rotor speed control with varying outer rotor torque reference

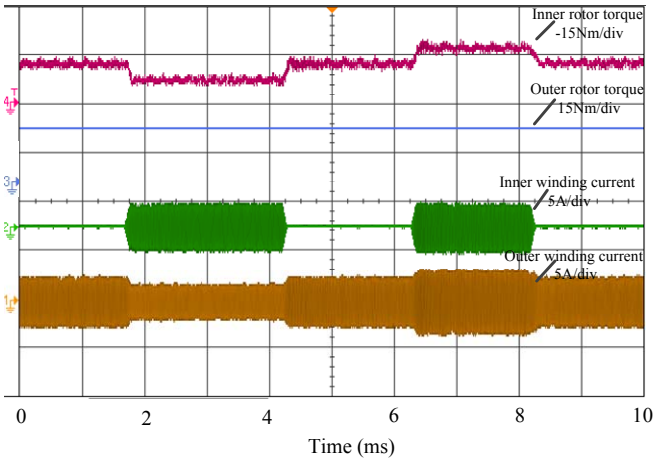

Fig. 14. Simulation results of power splitting and combination with constant load torque and varying winding currents.

V. Conclusion

In this paper, a novel structure of DR-FBMM is proposed for the E-CVT system of the HEV. It is an alternative solution with gearless and brushless structure for the HEV application. The mathematical model is derived and verified by the FEM simulation results. The simulation results also prove the effectiveness of this structure for the E-CVT application. The DR-FBMM employs the flux modulation effect to realize the power splitting and combination between the two rotors. An additional winding is integrated on the stator and coupled with the middle rotor. The additional winding can enhance the output torque of the wheels or work as generator to charge the battery. The control strategy of the novel structure is designed and testified by simulation results. The prototype of the machine is fabricated based on the optimization result of the FEM. The experiment results show the effectiveness of the mathematical model and FEM simulations.

Both simulation and experimental results show that the DR-FBMM is a promising option for the E-CVT system of HEV.

VI. References

[1] K. T. Chau, C. C. Chan, and C. Liu, "Overview of permanent-magnetbrushless drives for electric and hybrid electric vehicles," *IEEE Trans.Ind. Electron.,* vol. 55, no. 6, pp. 2246–2257, Jun. 2008.

[2] B. Mashadi and S. A. M. Emadi, "Dual-mode power-split transmission for hybrid electric vehicles", *IEEE Trans. Veh. Technol.*, vol. 59, no. 7, pp. 3223-3232, 2010.

[3] E. Vinot, R. Trigui, Y. Cheng, C. Espanet, A. Bouscayrol and V. Reinbold, "Improvement of an EVT-based HEV using dynamic programming," *IEEE Trans. Veh. Technol.,* vol. 63, no. 1, pp. 40–50, Jan. 2014.

[4] Y. Cheng, R. Trigui, C. Espanet, A. Bouscayrol, and S. Cui, "Specifications and design of a PM electric variable transmission for Toyota Prius II," IEEE Trans. Veh. Technol., vol. 60, no. 9, pp. 4106–4114, Nov. 2011.

[5] J. M. Miller, "Hybrid electric vehicle propulsion system architectures of the e-CVT type," *IEEE Trans. Power Electron.,* vol. 21, no. 3, pp. 756–767, May 2006.

[6] K. van Berkel, T. Hofman, B. Vroemen, and M. Steinbuch, "Optimal control of a mechanical-hybrid powertrain," *IEEE Trans. Veh. Technol.,* vol. 61, no. 2, pp. 485–497, Feb. 2012.

[7] B. Mashadi and S. A. M. Emadi, "Dual-mode power-split transmission for hybrid electric vehicles," IEEE Trans. Veh. Technol., vol. 59, no. 7, pp. 3223–3232, Sep. 2010.

[8] A. Ghayebloo and A. Radan, "Superiority of Dual-Mechanical-Port-Machine-Based Structure for Series–Parallel Hybrid Electric Vehicle Applications", *IEEE Trans. Veh. Technol.,* On page(s): 589 - 602 Volume: 65, Issue: 2, Feb. 2016.

[9] S. Niu, S. L. Ho and W. N. Fu, "A novel double-stator double-rotor brushless electrical continuously variable transmission system", *IEEE Trans. Magn.*, vol. 49, no. 7, pp. 3909-3912, 2013.

[10] A. Dalal, M. Ansari and P. Kumar, "A novel steady state model of a hybrid dual rotor motor comprising electrical equivalent circuit and performance equations", *IEEE Trans. Magn.*, vol. 50, no. 12, 2014.

[11] K. T. Chau, D. Zhang, J. Z. Jiang, C. Liu and Y. Zhang, "Design of a magnetic-geared outer-rotor permanent-magnet brushless machine for electric vehicles", *IEEE Trans. Magn.*, vol. 43, no. 6, pp. 2504-2506, 2007.

[12] P. Zheng, Q. Wu, J. Zhao, C. Tong, J. Bai and Q. Zhao, "Performance analysis and simulation of a novel brushless double rotor machine for power-split HEV applications", *Energies*, vol. 5, no. 1, pp. 119-137, 2012.

[13] S. Niu, S. L. Ho and W. N. Fu, "A novel double-stator double-rotor brushless electrical continuously variable transmission system", *IEEE Trans. Magn.*, vol. 49, no. 7, pp. 3909-3912, 2013.

[14] S. L. Ho, S. Niu, and W. N. Fu, "Design and Comparison of Vernier Permanent Magnet Machines", *IEEE Trans. On Magnetics,* Vol. 47, No. 10, 2011, pp. 3280-3283.

[15] J. Li, D. Wu, X. Zhang and S. Gao, "A New Permanent Magnet Vernier In-Wheel Motor for Electric Vehicles", *Vehicle Power and Propulsion Conference (VPPC)*, 2010, pp. 1-6.

[16] C.H. Lee, "Vernier Motor and Its Design", " I*EEE Trans. Power App. Syst.,* vol. 82, no. 66, pp. 343–349, Jun. 1963.

[17] K. Atallah, S. D. Calverley, and D. Howe, "Design, analysis and realisation of a high-performance magnetic gear," *Proc. Inst. Elect. Eng.—Elect. Power Appl.,* vol. 151, no. 2, pp. 135–143, Mar. 2004.

[18] R. Qu, D. Li, J. Wang, "Relationship Between Magnetic Gears and Vernier Machines", *Electrical Machines and Systems (ICEMS)*, 2011 International Conference on, 2011, pp. 1-6.

[19] J. Bai, P. Zheng, C. Tong, Z. Song and Q. Zhao, "Characteristic analysis and verification of the magnetic-field modulated brushless double-rotor machine", *IEEE Trans. Ind. Electron.,* vol. 62, no. 7, pp. 4023–4033, Jul. 2015.

[20] L. Sun, M. Cheng, and H. Jia, "Analysis of a novel magnetic-geared dual rotor motor with complementary structure, " *IEEE Trans. Ind. Electron.,* vol. 62, no. 11, pp. 6737–6747, Nov. 2015.

[21] B. Kim and T. A. Lipo, "Operation and Design Principles of a PM Vernier Motor", *IEEE Trans. On Industry Applications.,* Vol. 46 , No. 6, 2014, pp. 3656-3663